Computer-Aided Performance Evaluation of a Multichannel Transcranial Magnetic Stimulation System

Chang-Hwan Im[1,2] and Chany Lee[3]

[1]Department of Biomedical Engineering, Yonsei University, Wonju, Kwangwon-do 220-710 Korea
[2]Institute of Medical Engineering, Yonsei University, Wonju, Republic of Korea
[3]School of Electrical Engineering and Computer Science, Seoul National University, Seoul 151-742, Korea

We have evaluated a multichannel transcranial magnetic stimulation (TMS) system using realistic simulations based on the boundary element method (BEM). We investigated various configurations and types of stimulation coils by means of quantitative measures such as targeting accuracy and field concentration. The simulation studies applied to four different head-brain models suggest improved coil types yielding enhanced targeting accuracy and concentrated evoked electric field distribution.

***Index Terms*—Boundary element method (BEM), magnetic brain stimulation, transcranial magnetic stimulation (TMS).**

I. Introduction

External time-varying magnetic field can induce electrical current flow (eddy current) inside conductive human body tissues. The current flow then stimulates neurons electrically, which can be potentially used for neuronal rehabilitation [1]–[9]. When the time-varying magnetic field is used to stimulate brain cortical neurons, such a brain stimulation system is generally called a transcranial magnetic stimulation (TMS) system. The TMS system has many clinical and neuroscience applications because it is less invasive and less painful than electrical brain stimulation, which injects electrical currents directly on the scalp surface [3], [8], [9]. It can be used to verify functions of specific brain regions or to control basic human actions. Previous studies have shown that TMS is also promising for curing neuro-psychiatric or central-nervous-system diseases, such as depression, Parkinson's disease, epilepsy, and so on [9], [10].

Early studies on the magnetic stimulation used a single ring-type or figure-eight coil [1]–[5], but nowadays multichannel magnetic stimulation has been drawing interest [6]–[8]. Using multiple independently controlled stimulating coils, one can stimulate multiple loci in one shot, or with short delay between the pulses. The operator can also alleviate the nuisance caused by the activation of undesired structures by suppressing the field at selected locations. Moreover, it is possible to quickly scan brain regions since the coils do not need to be moved during scanning. The use of multiple coils improves the mapping resolution since the stimulating field can be made more concentrated [6].

Previous studies on the multichannel magnetic stimulation systems, however, assumed simple coil configurations such as planar and hemispherical arrangements. Moreover, they assumed simple head models such as free-space or cylindrical conductor to evaluate evoked electric field inside conductive tissues [6]–[8]. To the best of our knowledge, however, analysis of a practical whole-head TMS system based on realistic simulations has not been studied yet. In the present study, three different coil configurations and four different coil types were simulated adopting the boundary element method (BEM), which can consider realistic volume current conduction inside a human head. Cortical surface model extracted from four human subjects' magnetic resonance (MR) images were used, for the first time, to investigate evoked current patterns on cortical pyramidal neurons. The simulation results were compared and analyzed by means of quantitative measures such as targeting accuracy and field concentration. From the simulation studies, we could find more appropriate coil configurations and types yielding enhanced targeting accuracy and focalized evoked current distribution.

II. Methods

TMS is an inverse process of magnetoencephalography (MEG), which is a kind of noninvasive brain mapping technique that reconstructs brain electrical sources on the human cerebral cortex using external magnetic field recordings [11]. Thus, we can calculate the TMS-evoked current on the cortex based on the reciprocal relationship between MEG and TMS [6]–[8].

A. Determination of Optimal Coil Currents

The relationship between the evoked electric field $\mathbf{E}$ and time-varying external currents in the multichannel TMS coils is defined approximately as follows by virtue of the reciprocal characteristic between MEG and TMS [6]–[8]:

$$\mathbf{E}(\mathbf{r}) = \sum_{i=1}^{n} (dI_i/dt) L_i(\mathbf{r}) \tag{1}$$

where n is the number of stimulating coils, $\mathbf{r}$ is a point to calculate the evoked electric field vector $\mathbf{E}(\mathbf{r})$, dI_i/dt is the time derivative of current in ith coil, and L_i $(\mathbf{r})$ represents magnetic flux density at ith TMS coil induced by a unit dipolar current

Digital Object Identifier 10.1109/TMAG.2006.883913

source located at the position $\mathbf{r}$, of which the concept is adopted from MEG thanks to the reciprocity theory [6]–[8]. Since most neurons (over 95%) which we want to stimulate using the proposed TMS system are located only on the very thin ($\sim$4 mm) gray matter of human cerebral cortex [12], [13], it is physiologically reasonable to restrict possible stimulating points only to the cortical surface extracted from MRI T1-weighted images. Assuming N points on the extracted cortical surface, (1) can be rewritten in the following matrix form:

$$\mathbf{E} = \mathbf{L}\mathbf{I}_t \tag{2}$$

where $\mathbf{I}_t$ represents the time derivatives of current at n TMS coils, and $\mathbf{E}$ is the evoked electric field vectors at N cortical surface points. In MEG, $\mathbf{L}$ is usually referred to as a leadfield matrix [10]. The size of $\mathbf{E}$ and $\mathbf{L}$ are $3N \times 1$ and $3N \times n$, respectively, where "3" represents the three basis directions of an electric field vector.

If we assume a certain evoked field pattern $\mathbf{P}$, of which the size is also $3N \times 1$, the optimal derivatives of current can be determined by solving a linear inverse problem with truncated singular value decomposition (tSVD) [6] as follows:

$$\mathbf{I}_t = \mathbf{L}^{+}\mathbf{P} \tag{3}$$

where $\mathbf{L}^{+}$ is the pseudo-inverse of the lead field matrix. Mutual coupling effect should be considered in the practical system design [7], which finds charge voltage of each coil, but in the present study we have no need to consider the effect since we directly used $\mathrm{d}I/\mathrm{d}t$ as a variable to evaluate induced electric field. The evoked electric field on the cortical surface can then be estimated by

$$\mathbf{E} = \mathbf{L}\mathbf{L}^{+}\mathbf{P}. \tag{4}$$

B. Construction of Lead Field Matrix Considering Realistic Volume Conduction

As mentioned above, conventional studies on the multichannel magnetic stimulation system assumed simple volume conduction models such as a free-space or a simplified volume conductor [6]–[8]. In this paper, we used the BEM to calculate forward solutions and construct the lead field matrix considering more realistic volume conduction effect [11], [14], [15]. As aforementioned, the leadfield matrix in (1) is exactly the same as that of MEG forward problem because of the reciprocity between MEG and TMS. Therefore, the leadfield matrix can be constructed by calculating magnetic flux density at ith TMS coil induced by a unit dipolar current source located at the position $\mathbf{r}$. If we assume that a head is composed of a set of contiguous regions with constant isotropic conductivity $\sigma_i, i = 1, \ldots, 4$, representing the brain, skull, scalp, and air for instance, we can derive, from the Biot–Savart law, a relationship between measured magnetic field $\mathbf{B}(\mathbf{r})$ and electric potential on the interfaces of adjacent regions $V(\mathbf{r}')$ as

$$\mathbf{B}(\mathbf{r}) = \mathbf{B}_0(\mathbf{r}) + \frac{\mu_0}{4\pi}\sum_{ij}(\sigma_i - \sigma_j)\int_{S_{ij}} V(\mathbf{r}')\frac{\mathbf{R}}{R^3} \times \mathbf{dS}'_{ij} \tag{5}$$

where $R = |\mathbf{R}| = |\mathbf{r} - \mathbf{r}'|$, S_{ij} is the interface surface between ith and jth regions, and the primed symbols refer to quantities on the interfaces. The $\mathbf{B}_0(\mathbf{r})$ is the magnetic flux density due to the primary current only. The second term is the volume current contributions to the magnetic field formed as a sum of surface integrals over the brain-skull, skull-scalp, and scalp-air boundaries. The $\mathbf{B}_0(\mathbf{r})$ can be evaluated as

$$\mathbf{B}_0(\mathbf{r}) = \frac{\mu_0}{4\pi}\int_G \mathbf{J}^p(\mathbf{r}') \times \frac{\mathbf{R}}{R^3} dv' \tag{6}$$

where G is a domain in which current sources exist and $\mathbf{J}^p(\mathbf{r})$ represents a primary current density at $\mathbf{r}$ and is assumed to be a dipolar source in the present study. If a dipolar source is located at $\mathbf{r}_Q$, the primary current can be expressed as

$$\mathbf{J}^p(\mathbf{r}) = \mathbf{Q}\delta(\mathbf{r} - \mathbf{r}_Q) \tag{7}$$

where $\delta(\mathbf{r})$ is the Dirac delta function and $\mathbf{Q}$ is called the dipole moment vector.

From (5), we can see that electric potentials on interfaces should be determined to calculate magnetic flux density at the measuring point $\mathbf{r}$. The interface potentials can be calculated by solving the following integral equation:

$$(\sigma_i + \sigma_j)V(\mathbf{r}) = 2\sigma_0 V_0(\mathbf{r}) + \frac{1}{2\pi}\sum_{ij}{}'(\sigma_i - \sigma_j)\int_{S_{ij}} V(\mathbf{r}')d\Omega_{\mathbf{r}}(\mathbf{r}') \tag{8}$$

where $\mathbf{r} \in S_{ij}$ and σ_0 is the unit conductivity $\sigma_0 = 1/(\Omega m)$. Note that $d\Omega_{\mathbf{r}}(\mathbf{r}') = -|\mathbf{r} - \mathbf{r}'|^{-3}(\mathbf{r} - \mathbf{r}') \cdot \mathbf{dS}'_{ij}$, is the solid angle subtended at $\mathbf{r}$ by the surface element $\mathbf{dS}'_{ij}$ at $\mathbf{r}'$. $V_0(\mathbf{r})$ is a primary potential due to the primary current in an infinite homogeneous medium with unit conductivity and can be expressed as

$$V_0(\mathbf{r}) = \frac{1}{4\pi\sigma_0}\int_G \frac{\nabla' \cdot \mathbf{J}^p(\mathbf{r}')}{R} dv'. \tag{9}$$

The magnetic flux density by the primary current can be evaluated using electric potential V at all boundary nodes after solving the discretized version of (8). It has been frequently reported that considering inner skull boundary is sufficient for the MEG forward calculations because of the skull insulation effect [14], [15]. In the present study, the inner skull boundary was extracted and tessellated from MRI T1-weighted images [12]. Fig. 1 shows an example of the tessellated boundary element model co-registered with a cortical surface model.

On the other hand, we restricted locations of target points only on the interface between white matter and gray matter of a subject's cerebral cortex. This constraint is physiologically plausible and practical because most neurons are located on the cortical surface (actually within a very thin gray matter), not inside of the white matter [12], [13]. The brain cortical surface was extracted from MRI T1-weighted image (256 × 256 × 200, voxel size for each direction: 1 mm) and tessellated into about 500 000 triangular elements. To extract and tessellate the cortical surface, we applied *BrainSuite* developed in University of Southern California [16]. The lead field matrix in (1) can then be evaluated by assuming unit dipolar sources at each point on

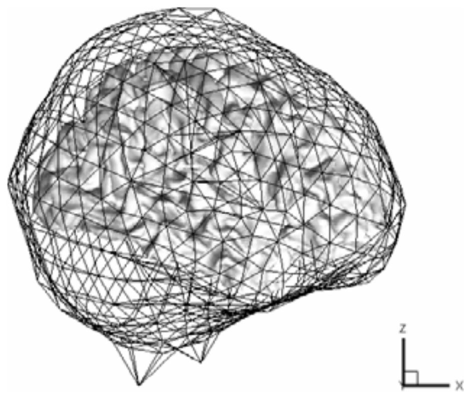

Fig. 1. Example of boundary element mesh on inner skull boundary. Some pyramids at the inferior side of the surface were generated because of inhomogeneity in structural MRI data.

the cortical surface and calculating magnetic field at all coil locations. We used four human subjects' structural MRI data with different sizes and shapes. Fig. 2 shows the four cortical surface models used to verify the performance of the designed TMS systems. Note that we applied different coil types and configurations to all the subjects, but presented the results only for subject #1 except for the quantitative comparison study. In the comparison study, we averaged the evaluated measures of all subjects.

III. Simulations and Results

We performed several simulations for four different types and three different configurations of stimulating coils and investigated the targeting accuracy and field concentration.

A. Simulation Setups

Before the simulations, target points should be assumed *a priori*. When a target point is selected among the vertices on the tessellated cortical surface, the desired evoked field pattern $\mathbf{P}$ in (2) is determined. The vector $\mathbf{P}$ has the only nonzero values at the target point. The directions of the targeted electric fields were assumed to be normal to the cortical surface since major pyramidal neurons which we would like to stimulate are arranged perpendicularly to the cortical surface [11], [12]. For example, a unit normal vector at a cortical surface point i is (Q_{xi}, Q_{yi}, Q_{zi}), the $\mathbf{P}$ vector was set as $(0, 0, \ldots, 0, Q_{xi}, Q_{yi}, Q_{zi}, 0, 0, \ldots, 0, 0)$. The evoked electric field at every cortical vertex was then evaluated using (4).

B. Multichannel TMS Systems

We simulated three different coil configurations. The proposed 61-channel, 102-channel, and 148-channel TMS systems were designed to cover upper side of a normal human brain. The coils were placed as regularly as possible to get consistent characteristics at all brain areas. The size of each coil and covering area of the whole system were consistent in every case. Fig. 3 shows the designed helmet-type whole head stimulators co-registered with subject #1's cortical surface.

Conventional stimulating coils that have been used for multichannel TMS were single coils normal to the coil surface as shown in Fig. 4(a) [8], which was named **Type 0** coil. In the present study, three more coil types were simulated, as depicted

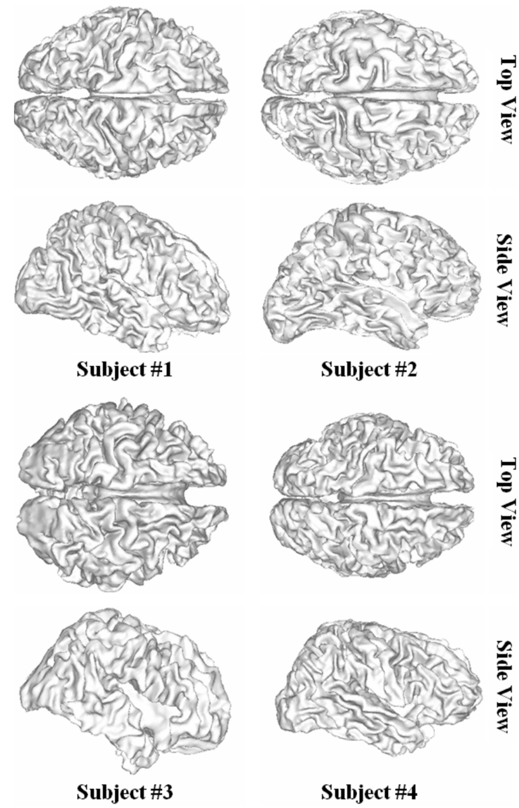

Fig. 2. Cortical surfaces extracted and tessellated from four subjects' MRI data—top views and side views.

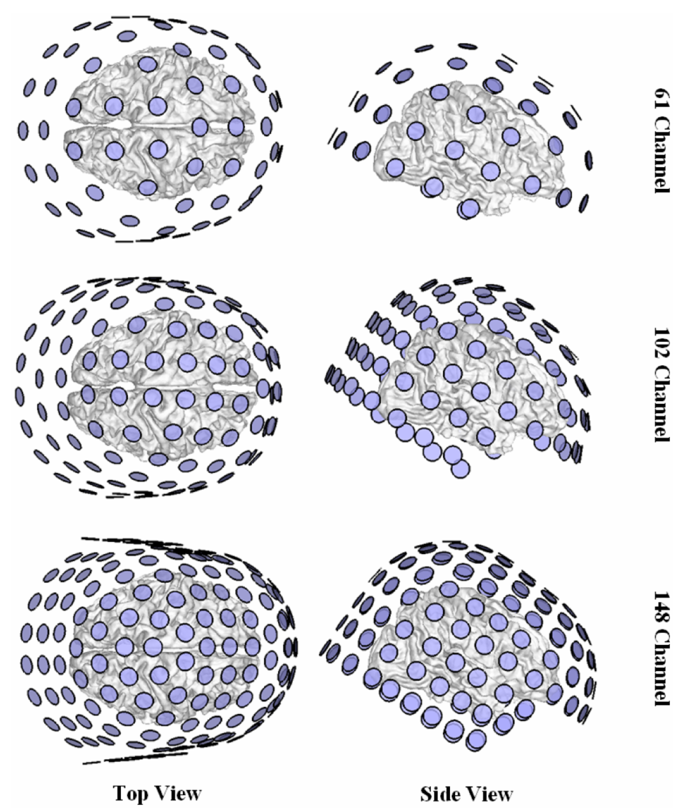

Fig. 3. Three different configurations of TMS coils—61, 102, and 148 coils from top to bottom. The coils were placed as regularly as possible to get consistent accuracy at all brain areas. (Color version available online at http://ieeexplore.ieee.org.)

in Fig. 4(b)–(d). The **Type 1** coil consisted of two orthogonal coils which are normal to the coil surface. The **Type 2** coil consisted of three orthogonal coils, which is a combination of **Type 0** and **Type 1**. The **Type 3** coil consisted of two parallel **Type 0** coils, which are working independently. The distance between the two coils was set to be 8 mm, which was determined after some trial and error processes to maximize targeting accuracy. In total, 48 different cases (3 coil configurations $\times$ 4 coil types $\times$ 4 subjects) were simulated and analyzed by means of two quantitative measures which will be introduced in the following section.

C. Quantitative Assessment of the System Performance 1: Targeting Accuracy

The most important issue of TMS is to accurately match the maximum of evoked field distribution to a target point on cortical surface. In the present study, we first defined a targeting error at ith node of cortical surface as the distance between the target point (ith node) and a maximal point of evoked field distribution. After evaluating errors at entire cortical vertices by changing the positions of the target point, we could construct a targeting error map on the cortical surface. Investigating the error map, we could estimate goodness of a TMS system intuitively. Fig. 5(a)–(c) shows examples of error maps calculated for 61-, 102-, and 148-channel configurations with **Type 0** coil, where the brighter region represents relatively the higher error. It could be observed from the figures that deep brain regions could not be stimulated well by external magnetic stimulations as insisted in previous literatures [1], [6]. The use of more coils could reduce area of higher error regions as expected.

In practical applications, the targeting errors in deep regions can be neglected since current applications of TMS generally concern sensory-related brain activations that occur around shallow cortical areas. Therefore, we excluded the deep points of which the depth from inner skull boundary exceeded 40 mm. An arithmetic mean of overall errors was then evaluated only at shallow cortical locations, for quantitative comparisons.

Fig. 6 shows the mean of the targeting errors evaluated with respect to all possible combinations of coil configurations and types and averaged for four different cortical surface models. The results demonstrate that **Type 2** coil shows the best performance among all coil types considered, but we should note that the number of coils used in **Type 2** is three times more than that of **Type 0**. Considering the number of coils used in **Type 2** (1.5 times more than **Type 3**), the enhancement in targeting error does not seem sufficient. Comparing the mean errors between **Type 1** and **Type 3**, of which the number of coils is twice more than that of **Type 0**, **Type 3** shows better performance than **Type 1**. Interestingly, the error of **Type 3** is comparable to that of **Type 2** in spite of large difference in the number of coils. Moreover, the error of **Type 3** in 61-channel configuration (total number of coil is only 122) is even superior to that of **Type 0** in 148-channel configuration. Thus, we can conclude that the **Type 3** coil (two axially parallel coils) is the best coil configuration for the multichannel whole head TMS system, from the viewpoint of targeting error.

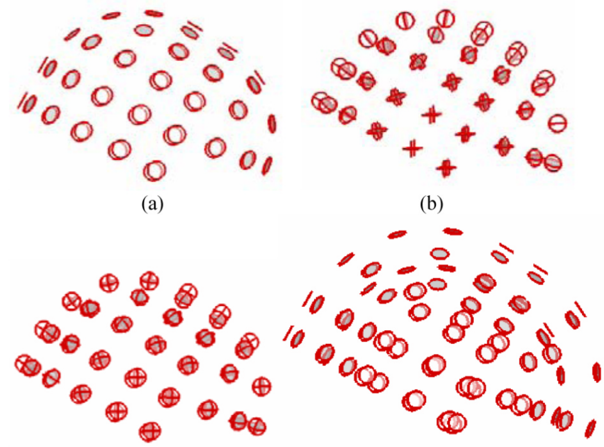

Fig. 4. Four different coil types applied to 61 coil configuration: (a) **Type 0** coil—conventional coil type; (b) **Type 1** coil—two orthogonal coils perpendicular to coil surface; (c) **Type 2** coil—combination of **Type 0** and **Type 1** coils; (d) **Type 3** coil—two parallel **Type 0** coils. (Color version available online at http://ieeexplore.ieee.org.)

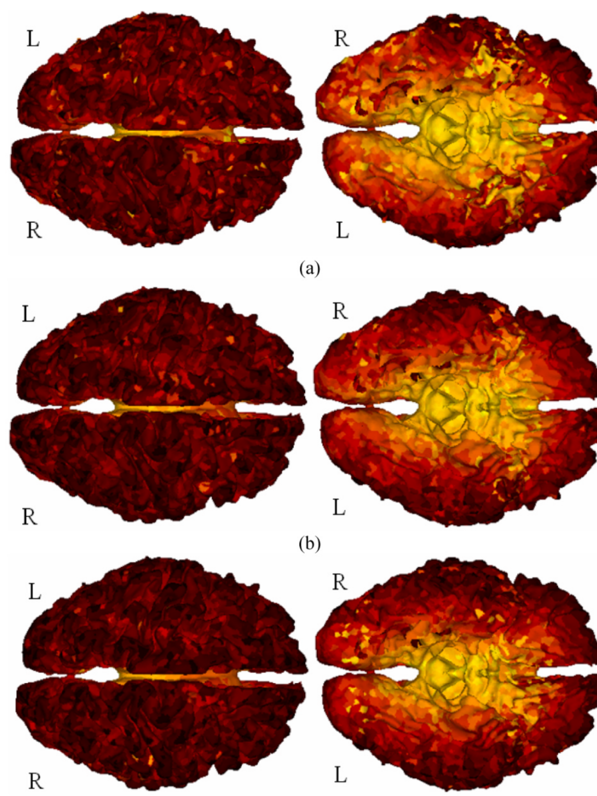

Fig. 5. Examples of error maps calculated for 61-, 102-, and 148-channel configurations with **Type 0** coil (tested on subject #1's cortical surface), where the brighter region represents relatively the higher error: (a) 61-channel; (b) 102-channel; (c) 148-channel. Left figures are top view and right figures are bottom view. "R" represents right side and "L" represents left side. All values were normalized with respect to 25 mm for relative comparison. (Color version available online at http://ieeexplore.ieee.org.)

D. Quantitative Assessment of the System Performance 2: Field Concentration

Level of evoked field concentration should be another important measure to assess the performance of a TMS system. To

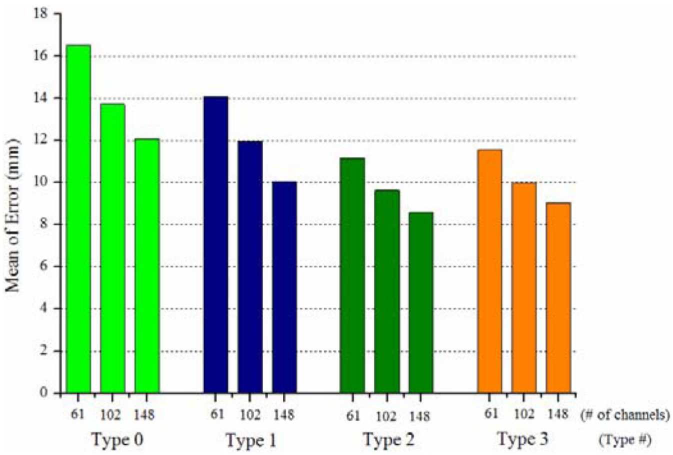

Fig. 6. Mean of the targeting errors (unit: mm) evaluated for all possible combinations of coil configurations and types (averaged for four head-brain models). 61, 102, and 148 represent the number of channels. (Color version available online at http://ieeexplore.ieee.org.)

quantify the field concentration at ith node of cortical surface, we calculated the total area of cortical patches (triangular elements), of which the evoked field strengths exceeded half of the maximum evoked field. After evaluating the areas (or extensions) at entire cortical vertices by changing the positions of the target point, we could also construct a field concentration map on the cortical surface. The map could give us another intuitive measure to estimate goodness of a TMS system. Fig. 7(a)–(c) shows examples of the field concentration maps calculated for 61-, 102-, and 148-channel configurations with **Type 0** coil, where the brighter region represents relatively the wider evoked field distribution. It can be also seen from the figures that one can obtain more focalized evoked field distributions by using more coils.

Fig. 8 shows the mean of the field concentration evaluated with respect to all possible combinations of coil configurations and types and averaged for four different cortical surface models. As in the targeting error evaluation, we excluded deep cortical areas of which the depth from inner skull boundary exceeded 40 mm. The results demonstrate that the field concentration of **Type 3** coil is comparable with that of **Type 2** coil despite of even less number of coils. As in the previous investigation, the **Type 3** coil showed the best performance among all types of coils. We can observe that the averaged field concentration of **Type 3** in 61-channel configuration (total number of coil is only 122) is even superior to that of **Type 0** in 148-channel configuration.

In summary of the two quantitative comparison studies, we could conclude that the axially parallel coil type **(Type 3)** shows the best performance in both targeting error and level of field concentration.

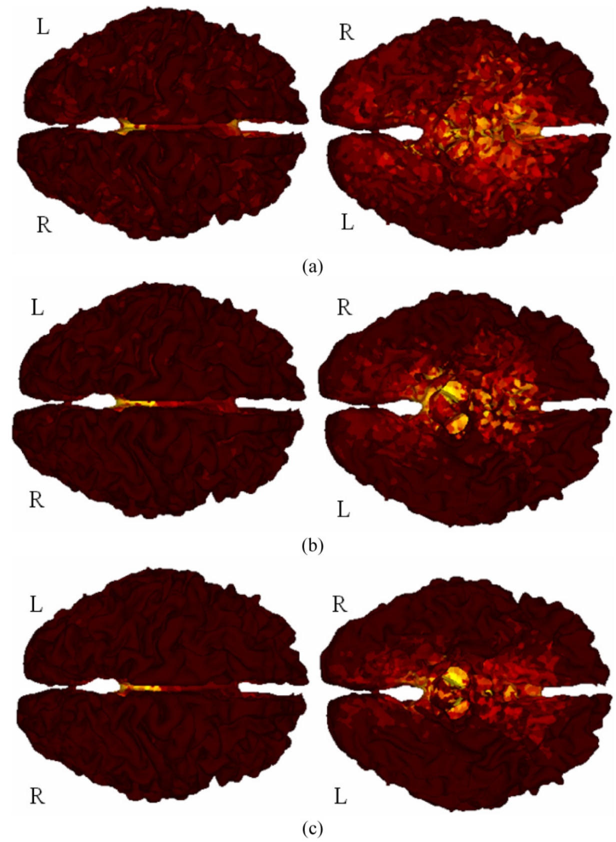

Fig. 7. Examples of field concentration maps evaluated for 61-, 102-, and 148-channel configurations with **Type 0** coil (tested on subject #1's cortical surface), where the brighter region represents relatively the wider evoked field distribution: (a) 61-channel; (b) 102-channel; (c) 148-channel. Left figures are top view and right figures are bottom view.'R' represents right side and 'L' represents left side. All values were normalized with respect to 5×10^4 mm^2 for relative comparisons. (Color version available online at http://ieeexplore.ieee.org.)

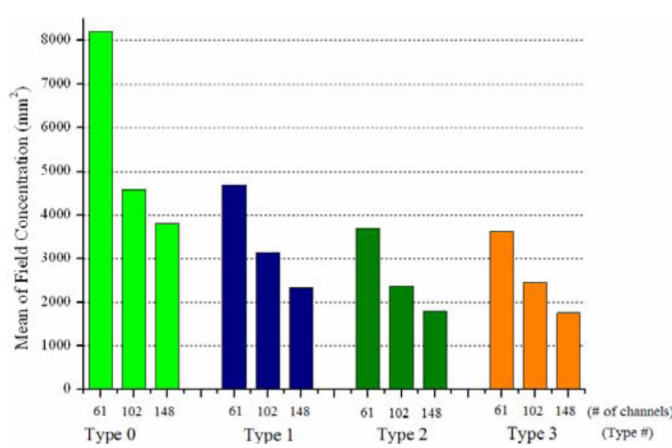

Fig. 8. Mean of the field concentration (unit: mm^2) evaluated for all possible combinations of coil configurations and types (averaged for four head-brain models). 61, 102, and 148 represent the number of channels. (Color version available online at http://ieeexplore.ieee.org.)

IV. Conclusion

In the present study, we evaluated a multichannel whole-head TMS system considering realistic head-brain geometry. We tested various types and configurations of stimulating coils utilizing boundary element method (BEM). The targeting errors and field concentration levels with respect to the configurations and types of coils were investigated by means of quantitative measures. The extensive simulation studies demonstrated that the use of axially parallel coil type can not only enhance targeting accuracy, but also focalize evoked field distribution. It is expected that the results of this conceptual design and the methodologies used in the present study will be a useful guide to realize human *in vivo* experimental systems. Further studies will be continued to predict more accurate induced electric field distributions using 3-D eddy-current analysis and to investigate electric power consumption and threshold voltage for manufacturing purpose.

ACKNOWLEDGMENT

This work was supported by a grant from the Korea Health 21 R&D project, Ministry of Health and Welfare, Korea (02-PJ3-PG6-EV07-0002).

REFERENCES

[1] J. Ruohonen, M. Ollikainen, V. Nikouline, J. Virtanen, and R. J. Ilmoniemi, "Coil design for real and sham transcranial magnetic stimulation," *IEEE Trans. Biomed. Eng*, vol. 47, no. 2, pp. 145–148, Feb. 2000.
[2] J. Starzyński, B. Sawicki, S. Wincenciak, A. Krawczyk, and T. Zyss, "Simulation of magnetic stimulation of the brain," *IEEE Trans. Magn.*, vol. 38, no. 2, Mar. 2002.
[3] S. Ueno, "Biomagnetic approaches to studying the brain," *IEEE Eng. Med. Biol. Mag.*, vol. 18, no. 3, pp. 108–120, May–Jun. 1999.
[4] K. Iramina, T. Maeno, and S. Ueno, "Topography of EEG responses evoked by transcranial magnetic stimulation to the cerebellum," *IEEE Trans. Magn.*, vol. 40, no. 4, pp. 2982–2984, Jul. 2004.
[5] K. Davey and M. Riehl, "Designing transcranial magnetic stimulation systems," *IEEE Trans. Magn.*, vol. 41, no. 3, pp. 1142–1148, Mar. 2005.
[6] J. Ruohonen, P. Ravazzani, F. Grandori, and R. J. Ilmoniemi, "Theory of multichannel magnetic stimulation: Toward functional neuromuscular rehabilitation," *IEEE Trans. Biomed. Eng.*, vol. 46, no. 6, pp. 646–651, Jun. 1999.
[7] B.-H. Han, I.-K. Chun, S.-C. Lee, and S.-Y. Lee, "Multichannel magnetic stimulation system design considering mutual couplings among the stimulation coils," *IEEE Trans. Biomed. Eng.*, vol. 51, no. 5, pp. 812–817, May 2004.
[8] J. Ruohonen and R. J. Ilmoniemi, "Focusing and targeting of magneric brain stimulation using multiple coils," *Med. Biol. Eng. Comput.*, vol. 36, pp. 297–301, 1998.
[9] F. Binkofski, J. Classen, and R. Benecke, "Stimulation of peripheral nerves using a novel magnetic coil," *Muscle Nerve*, vol. 22, pp. 751–757, 1999.
[10] M. Walpoth, C. Hortnagl, J. Hinterholzl, A. Conca, H. Hinterhuber, and A. Hausmann, "Neuropsychiatric aspects of transcranial magnetic stimulation (TMS)," *Neuropsychiatrie*, vol. 19, pp. 3–14, 2005.
[11] M. S. Hamalainen, R. Hari, R. J. Ilmoniemi, J. Knuutila, and O. V. Lounasmaa, "Magnetoencephalography. Theory, instrumentation and applications to the noninvasive study of human brain function," *Rev. Mod. Phys.*, vol. 65, pp. 413–497, 1993.
[12] C.-H. Im, H.-K. Jung, and N. Fujimaki, "fMRI constrained MEG source imaging and consideration of fMRI invisible sources," *Hum. Brain Mapp.*, vol. 26, no. 2, pp. 110–118, 2005.
[13] A. M. Dale and M. Sereno, "Improved localization of cortical activity by combining EEG and MEG with MRI surface reconstruction: a linear approach," *J. Cognit. Neurosci.*, vol. 5, pp. 162–76, 1993.
[14] M. S. Hamalainen and J. Sarvas, "Realistic conductivity geometry model of the human head for interpretation of neuromagnetic data," *IEEE Trans. Biomed. Eng.*, vol. 36, pp. 165–171, 1989.
[15] J. W. Meijs, M. J. Peters, H. B. Boom, and F. H. Lopes da Silva, "Relative influence of model assumptions and measurement procedures in the analysis of the MEG," *Med. Biol. Eng. Comput.*, vol. 26, pp. 136–142, 1988.
[16] D. W. Shattuck and R. M. Leahy, "BrainSuite: An automated cortical surface identification tool," *Med. Image. Anal.*, vol. 6, pp. 129–142, 2002.

Manuscript received June 15, 2006; revised August 30, 2006. Corresponding author: C.-H. Im (e-mail: ich@yonsei.ac.kr).

Chang-Hwan Im graduated from the School of Electrical Engineering and Computer Science, Seoul National University, Seoul, Korea, in 1999. He received the M.S. and Ph.D. degrees from the same university in 2001 and 2005, respectively.

He worked as a Postdoctoral Associate in the Department of Biomedical Engineering, University of Minnesota, from 2005 to 2006. Since 2006, he has been an Assistant Professor in the Department of Biomedical Engineering, Yonsei University, Wonju, Korea. His research interests cover the various fields of bioelectromagnetics, especially multimodal neuronal source imaging, electrical impedance tomography, EEG/MEG/MCG forward/inverse problem, and transcranial magnetic stimulation (TMS).

Chany Lee was born in Taegu, Korea, in 1980. He graduated from the School of Electrical Engineering, Seoul National University, Seoul, Korea, in 2003. He received the M.S. degree from the same university in 2005. He is now working toward the Ph.D. degree in the school of Electrical Engineering and Computer Science, Seoul National University.

His research interests are bioelectromagnetics and transcranial magnetic stimulation.